Atmospheric
Measurement
Techniques

Profiling the PM$_{2.5}$ mass concentration vertical distribution in the boundary layer

Zongming Tao[1,2], Zhenzhu Wang[2], Shijun Yang[1], Huihui Shan[1], Xiaomin Ma[1], Hui Zhang[1], Sugui Zhao[1], Dong Liu[2], Chenbo Xie[2], and Yingjian Wang[2,3]

[1]New Star Institute of Applied Technology, Hefei, Anhui 230031, China
[2]Key Laboratory of Atmospheric Composition and Optical Radiation, Anhui Institute of Optics and Fine Mechanics, Chinese Academy of Sciences, Hefei, Anhui 230031, China
[3]University of Science and Technology of China, Hefei, Anhui 230031, China

Correspondence to: Zhenzhu Wang (zzwang@aiofm.ac.cn)

Abstract. Fine particles (PM$_{2.5}$) affect human life and activities directly; the detection of PM$_{2.5}$ mass concentration profile is very essential due to its practical and scientific significance (such as the quantification of air quality and its variability as well as the assessment of improving air quality forecast). But so far, it has been difficult to detect PM$_{2.5}$ mass concentration profile. The proposed methodology to study the relationship between aerosol extinction coefficient and PM$_{2.5}$ mass concentration is described, which indicates that the PM$_{2.5}$ mass concentration profile could be retrieved by combining a charge-coupled device (CCD) side-scatter lidar with a PM$_{2.5}$ sampling detector. When the relative humidity is less than 70 %, PM$_{2.5}$, mass concentration is proportional to the aerosol extinction coefficient, and then the specific coefficient can be calculated. Through this specific coefficient, aerosol extinction profile is converted to PM$_{2.5}$ mass concentration profile. Three cases of clean night (on 21 September 2014), pollutant night (on 17 March 2014), and heavy pollutant night (on 13 February 2015) are studied. The characteristics of PM$_{2.5}$ mass concentration profile at the near-ground level during the cases of these 3 nights in the western suburb of Hefei city were discussed. The PM$_{2.5}$ air pollutant concentration is comparatively large close to the surface and varies with time and altitude. The experiment results show that the CCD side-scatter lidar combined with a PM$_{2.5}$ detector is an effective and new method to explore pollutant mass concentration profile at the near-ground level.

1 Introduction

Atmospheric aerosol is defined as suspended particle in the air, and its size distributes from 0.001 to 100 µm in diameter in liquid or solid state. Fine particles (PM$_{2.5}$) constitute a particular group of particle, whose size is less than 2.5 µm in diameter; it is an important part of aerosol. PM$_{2.5}$ are also called fine particles because of their small size. PM$_{2.5}$ is considered to be the most serious pollutant in the urban areas all over the world due to its adverse health effects, including cardiovascular diseases, respiratory irritation, and pulmonary dysfunction (An et al., 2000; Mao et al., 2002; Xu et al., 2007). The PM$_{2.5}$ poses great health risks, compared to the coarse particle matter, because the increased surface areas have a high potential to adsorb or condense toxic air pollutants (An et al., 2000). Meanwhile PM$_{2.5}$ can degrade the atmospheric visibility and affect traffic safety by the extinction effect. In recent years, a series of experiments or monitors about fine particle matter are researched in many mega cities in China by institutes (Mao et al., 2002; Che et al., 2015), and the results indicated that the PM$_{2.5}$ mass concentration was increased.

Precise knowledge on the vertical distribution of PM$_{2.5}$ is required for at least two reasons: (1) it is better for quantifying air quality and its variability since, for example, the different vertical distribution of PM$_{2.5}$ near the Earth surface has very different impact on public health; (2) it is likely to significantly enhance the PM$_{2.5}$ estimation and provide data

information for model evaluation, improvement, and development for the daily air quality forecast.

Currently, the direct detecting device for PM$_{2.5}$ is the particle matter sampling monitor, which is mostly installed on the surface ground. Using the meteorological tower, only a few researchers fitted PM$_{2.5}$ monitors at different altitudes in Beijing and Tianjin to get the profile of PM$_{2.5}$ mass concentration within 325 m (Wu et al., 2009; Yang et al., 2005). So it is difficult to obtain PM$_{2.5}$ mass concentration profile in a few kilometers. However, some important atmospheric processes (i.e. particle formation, transportation and mixing processes) take place predominantly at a higher altitude in the planetary boundary layer. Lidar, in principle, can provide the ability to observe these processes where they occur. Backscattering lidar is a powerful tool to detect aerosol profile, and is widely used in atmospheric monitoring (Weitkamp, 2005; Winker et al., 2007; Bo et al., 2014; Wang et al., 2014b). But the common backscattering lidar system has a shortcoming in the lower hundreds of meters because of the geometric form factor (GFF) caused by the configuration of the transmitter divergence and receiver's field of view (FOV) at the near range (Mao et al., 2012; Wang et al., 2015b). With the recently developed technique of the CCD side-scattering lidar (Bernes et al., 2003; Tao et al., 2014a; Ma et al., 2014), the problem caused by the GFF could be solved. Moreover, the nearer range and the better spatial resolution could be obtained. So the side-scattering lidar is very suitable for detecting aerosol spatial distribution in the boundary layer from the surface.

In this paper, the aerosol extinction coefficient profile is retrieved by our self-developed CCD side-scattering lidar, and PM$_{2.5}$ mass concentration is measured simultaneously on the ground level by a particle matter monitor. Syncretizing these two data sets measured at the same time and in the same place, the profile of PM$_{2.5}$ mass concentration can be derived in the boundary layer. In Sect. 2, the instrumentation is introduced, and the methodology for extinction and PM$_{2.5}$ profiles is shown in Sect. 3. Then the results are discussed in Sect. 4, followed by the summary and conclusion in the last Sect. 5.

2 Instruments

The measurement system consists of a CCD side-scattering lidar and a PM$_{2.5}$ mass monitor as shown in Fig. 1. The subsystem of side-scattering lidar consists of laser, CCD camera, geometric calibration, data acquisition and control computer. The light source is a Nd : YAG laser (Quantel Brilliant) emitting laser pulses in 20 Hz at 532 nm wavelength. The side-scattering light is received by a CCD camera with 3352 × 2532 pixels. The exposed time is set as 5 min according to the signal-to-noise ratio with a maximum relative error of 1.5 % caused by noises (Ma et al., 2014), and there is an interference filter with 30 nm bandwidth in front of CCD lens. Through geometric calibration, the relationship
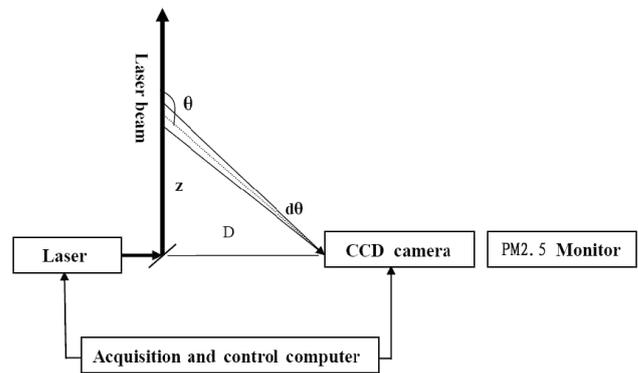

Figure 1. The diagram of the measurement system.

Table 1. The specifications of the C-lidar system.

Laser (Quantel Brilliant) Nd : YAG	
Wavelength (nm)	532
Pulse energy (mJ)	200
Repetition rate (Hz)	20
Detector (SBIG) ST-8300M	
Pixel array	3352 × 2532
Pixel size (μm)	5.4 × 5.4
A/D convecter (bits)	16
Wide-angle lens	Walimexpro f/2.8
Lens focal length (mm)	14
CCD sensor Kodak KAF-8300	
Quantum efficiency (532 nm)	∼ 55 %
Interference filter (Semrock corporation)	
Bandwidth (nm)	25.6
Peak transmittance	∼ 95 %

between the pixels and the corresponding scattering lights in laser beam is determined. The computer acquires the CCD camera data and controls timing sequence between laser and CCD camera. PM$_{2.5}$ mass monitor works simultaneously and the output is the average PM$_{2.5}$ mass concentration throughout 1 hour. In Fig. 1; z is the detecting distance; D is the distance from CCD camera to laser beam; θ is the scattering angle; dθ is the FOV of one pixel. The detailed specifications of the CCD side-scattering lidar (C-lidar) are described in the previous work (Tao et al., 2014a) and shown in Table 1.

The PM$_{2.5}$ mass monitor, named Thermo Scientific TEOM 1405 Ambient Particulate Monitor, can carry out continuous measurement of ambient particulate concentrations with the resolution of 0.1 μg m^3 and the precision of ±2.0 μg m^3 (1 hour averaged).

3 Methodology
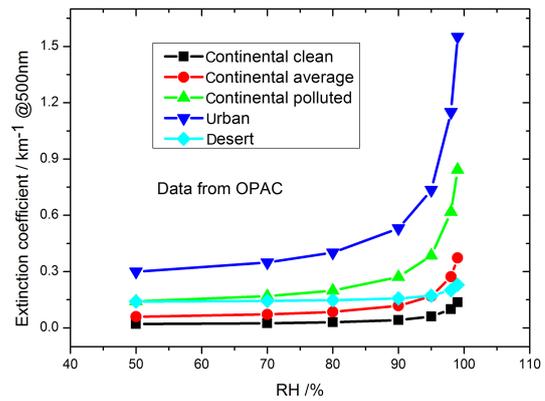
3.1 Retrieved method of aerosol extinction profile

The side-scattering lidar equation is expressed as (Tao et al., 2014b):

$$P(z, \theta) = \frac{P_0 K A}{D} \left(\frac{\beta_1(z, \pi)}{f_1(\pi)} f_1(\theta) + \frac{\beta_2(z, \pi)}{f_2(\pi)} f_2(\theta) \right) \qquad (1)$$
$$\times \exp \left(-\tau - \tau / \cos(\pi - \theta) \right) \mathrm{d}\theta,$$

where $P(z, \theta)$ is the received power at height z and scattering angle θ by a pixel, P_0 is laser pulse energy, K is a system constant including the optical and electronic efficiency, A is the area of CCD camera lens, D is the distance from CCD camera to laser beam, $\beta(z, \pi)$ is backscattering coefficient, and $f(\theta)$ is phase function. Subscripts "1" and "2" represent aerosol and molecule scattering, respectively. τ is optical depth, $\alpha(z)$ is extinction coefficient, and $\tau = \int_0^z (\alpha_1(z') + \alpha_2(z')) \mathrm{d}z'$.

In general, for Eq. (1), there are six unknown variables, i.e. phase function, backscattering and extinction coefficients of aerosol and molecule. Three unknown variables for molecule are calculated through the standard molecular model by Rayleigh scatter theory. A prior assumption has to be given, i.e. lidar ratio (extinction-to-backscattering ratio) of aerosol, because of the principle of lidar equation. The value of 50 Sr is used as lidar ratio at 532 nm wavelength in our algorithm. The aerosol phase function is determined from a sky-radiometer (for example, a Prede POM-02 sky-radiometer made in Japan). Then only one variable (the backscattering or extinction coefficient of aerosol) is left, which can be derived from Eq. (1) as follows.

In our experiment, vertical-pointing backscattering lidar (V-lidar) and C-lidar worked simultaneously. For V-lidar data processing, it is a traditional way to select the clear point about the tropopause as the reference point assumed to have minimum aerosol. The V-lidar signals and C-lidar signals have an overlap region around 1 km in height in our case. For C-lidar, the reference point is selected in this overlap region. Aerosol backscatter coefficient value β_c at the reference point thus can be given from V-lidar retrieval. When the aerosol backscatter coefficient value at the scattering angle θ_c as the reference point is known, according to Eq. (1), the backscattering or extinction coefficient of aerosol can be derived in our proposed numerical inversion method (Tao et al., 2014b). The validation experiments and error analysis are shown in the reference (Tao et al., 2015). When comparative experiments were performed, the C-lidar and V-lidar worked at the same position simultaneously, as well as another horizontal-pointing backscattering lidar (H-lidar). The result shown in the Fig. 2 of the reference (Tao et al., 2015) indicates a good agreement and the total relative error of extinction coefficient is less than 18 % accordingly in the error propagation method and by the typical example.

Figure 2. The relationship between aerosol extinction coefficient and atmospheric relative humidity (RH) for five types of aerosol.

3.2 Retrieved method of PM$_{2.5}$ profile

Some researchers (Pesch and Oderbolz, 2007; Sano et al., 2008; He et al., 2010; Cordero et al., 2012) studied the relationship between the PM$_{2.5}$ mass concentration and aerosol optical depth by a review of statistics. The aerosol optical depth is the integral result of aerosol extinction to range, which may match the column PM$_{2.5}$ mass concentration. However, the aerosol extinction and PM$_{2.5}$ mass concentration both change along altitude. So the PM$_{2.5}$ mass concentration is closely related to the aerosol extinction in theory.

The aerosol size distribution $n(r)$ is defined as

$$n(r) = \frac{\mathrm{d}N}{\mathrm{d}r}, \qquad (2)$$

where $\mathrm{d}N$ is the particle number concentration in radius interval range ($r \rightarrow r + \mathrm{d}r$).

Total particle matter mass concentration C_{Total} can be written as

$$C_{\text{Total}} = \int_0^\infty \rho \left(\frac{4}{3} \pi r^3 \right) n(r) \mathrm{d}r, \qquad (3)$$

where ρ is the aerosol mass density.

PM$_{2.5}$ mass concentration $C_{\text{PM}_{2.5}}$ can be written as

$$C_{\text{PM}_{2.5}} = \int_0^{2.5\,\mu\text{m}} \rho \left(\frac{4}{3} \pi r^3 \right) n(r) \mathrm{d}r. \qquad (4)$$

Aerosol extinction coefficient α can be described as

$$\alpha = \int_0^\infty \pi r^2 Q_{\text{ext}} n(r) \mathrm{d}r, \qquad (5)$$

where Q_{ext} is the factor of extinction efficiency.

The mean and integral properties of the particle ensemble that are calculated from the inverted particle size distribution

are effective radius, i.e. the surface-area-weighted mean radius as

$$r_{\text{eff}} = \int\limits_0^\infty r^3 n(r)\mathrm{d}r / \int\limits_0^\infty r^2 n(r)\mathrm{d}r. \qquad (6)$$

So, the relationship between aerosol extinction and total particle mass concentration is determined (Li et al., 2013)

$$\alpha = \frac{3Q_{\text{ext}}}{4r_{\text{eff}}\rho} C_{\text{Total}}. \qquad (7)$$

Using the ratio of total particle matter mass concentration to PM$_{2.5}$ mass concentration ($\eta = C_{\text{Total}}/C_{\text{PM}_{2.5}}$), finally we got the following relationship:

$$\alpha = \frac{3Q_{\text{ext}}\eta}{4r_{\text{eff}}\rho} C_{\text{PM}_{2.5}} = K \times C_{\text{PM}_{2.5}}. \qquad (8)$$

Eq. (8) is the formula to convert aerosol extinction profile to PM$_{2.5}$ mass concentration profile, where $K = \frac{3Q_{\text{ext}}\eta}{4r_{\text{eff}}\rho}$ is the specific coefficient.

In Eq. (8), the specific coefficient K is related to aerosol size distribution, refractive index, and atmospheric relative humidity. In the planetary boundary layer (PBL), due to turbulence effect, the aerosol size distribution and refractive index are assumed as to be reasonably uniform. When the relative humidity is below 70 %, the aerosol hydrophilic growth could be negligible. So, the specific coefficient K could be considered as constant under the condition of less than 70 % relative humidity in the PBL; i.e. K is independent of altitude, though this assumption will lead to limitation.

In a measurement, the CCD side-scattering lidar and PM$_{2.5}$ monitor operate in the same place simultaneously. After the aerosol extinction coefficient value corresponding to the altitude of PM$_{2.5}$ monitor and PM$_{2.5}$ mass concentration value is selected, the specific coefficient K is determined by Eq. (8). Then use Eq. (8) again, and the PM$_{2.5}$ mass concentration profile could be derived from aerosol extinction coefficient profile and the specific coefficient K.

4 Results

Our CCD side-scattering lidar system has been set up since April 2013 at the SKYNET Hefei site. After that, the system operated to detect atmospheric aerosol during cloud-free night. In the following, three cases are shown to represent clean day, pollutant day, and heavy pollutant day, respectively. Before this, in order to verify the prior assumption, we investigated how the aerosol extinction coefficient is associated with the atmospheric relative humidity (RH) through numerical calculation. The selected aerosol types for the calculation are shown in Fig. 2. The parameters and components for Fig. 2 were from the Optical Properties of Aerosols and Clouds (OPAC) 3.1 software by Hess et al. (1998). As mentioned in the previous literature (Wang et al., 2014a; 2015a),

the Hefei site is located in the east of China, which is predominantly continental aerosol. The nearest urban influence is 15 km; therefore, the site is close enough to be influenced by local urban aerosols depending on wind direction. And in spring, dust aerosol from the northern/northwest regions of China may also affect this site (Zhou et al., 2002). So, five different aerosol types are considered in Fig. 2, and they are rarely reliant on RH when RH is less than 70 %.

4.1 Case I: Clean night

On 21 September 2014, it was clear at night, with northeast wind of not more than 3 m s^{-1} near ground. The temperature ranges from 21.6 to 23.0 °C with a slight decreasing trend, and the RH increases from 61 to 69 % during the time span of 19:30–22:00 Beijing time (BT) as shown in Fig. 3a. The distance D between laser beam and CCD camera is 34.34 m.

Figure 3b plots the hourly mean value of K varying from 0.011 to 0.012 km^{-1} (µg m^{-3}), which indicates an approximately constant value during this experimental case. With the specific coefficient K and the aerosol extinction coefficient profile, PM$_{2.5}$ profile is given accordingly. Fig. 3c presents spatiotemporal distribution of PM$_{2.5}$ mass concentration for this case at the Hefei site. The PM$_{2.5}$ is almost enclosed below 1.5 km above ground level (a.g.l.) with a maximum value 33 µg m^{-3}, indicating a clean night in Hefei. The floating layer of 0.6–1.5 km a.g.l. indicates a higher PM$_{2.5}$, of which the value is more than that below 0.3 km a.g.l. near the Earth surface layer from Fig. 3c. The floating layer exists throughout the night due to a stable aerosol loading. There is a clean layer between the floating layer and the Earth surface layer. It is noted from Fig. 3d that the PM$_{2.5}$ value decreases from 28 µg m^{-3} on the Earth surface to 12 µg m^{-3} at 0.3 km a.g.l., and keeps at a certain value at 0.3–0.6 km a.g.l., and then increases to three sub-peaks of 29, 33, and 33 µg m^{-3} in the floating layer, respectively. The vertical distribution of PM$_{2.5}$ at 21:30 BT measured at the Hefei site on 21 September 2014 depicts a rich structure.

4.2 Case II: Pollutant night

On 17 March 2014, it was also clear at night, with the south wind of not more than 3 m s^{-1} near the Earth surface. The temperature varies from 18.2 to 21.7 °C with a decreasing trend and the RH increases from 58 to 70 % during the time span of 19:30–24:00 BT as shown in Fig. 4a. The distance D between laser beam and CCD camera is 23.90 m.

Figure 4b plots the hourly mean value of K varying around 0.011 km^{-1} (µg m^{-3}) with the minimum of 0.009 and the maximum of 0.012, which also indicates an approximately constant value during this experimental case. Then PM$_{2.5}$ profile is given accordingly by the specific coefficient K and the aerosol extinction coefficient profile. The spatiotemporal distribution of PM$_{2.5}$ mass concentration for this case at the Hefei site is shown in Fig. 4c. The PM$_{2.5}$ is almost enclosed
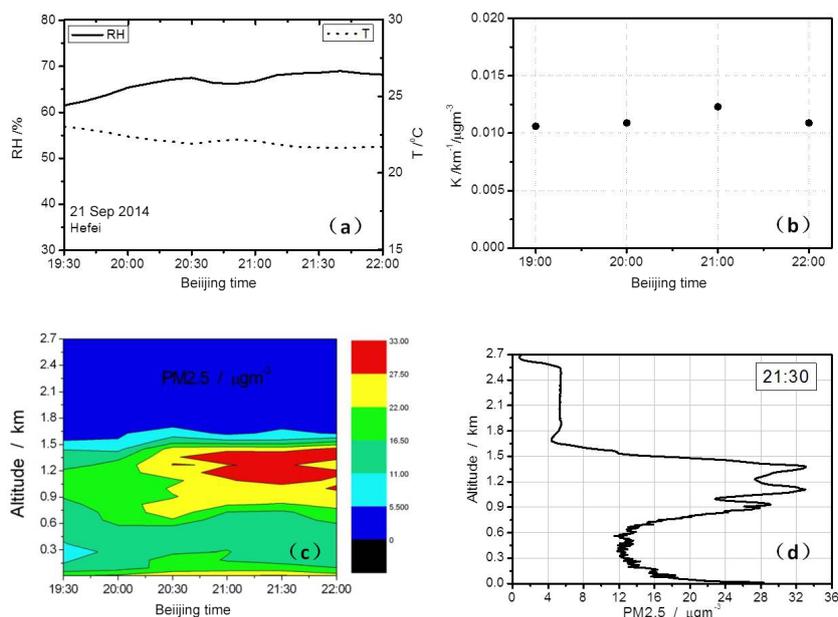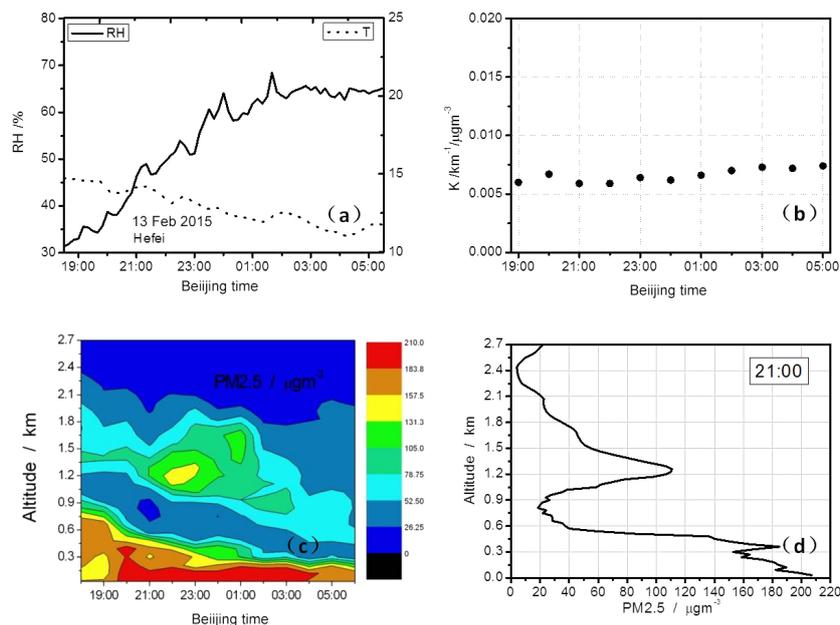
Figure 3. (a) RH and T parameters with time, **(b)** K value for each hour, **(c)** time series of PM$_{2.5}$ profile, and **(d)** vertical distribution of PM$_{2.5}$ at 21:30 BT measured at the Hefei site on 21 September 2014.
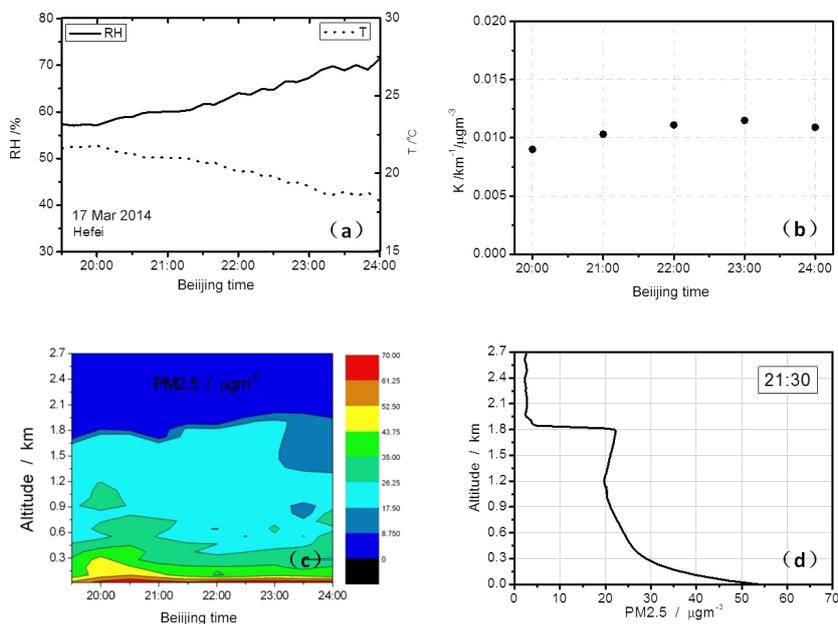
Figure 4. (a) RH and T parameters with time, **(b)** K value for each hour, **(c)** time series of PM$_{2.5}$ profile, and **(d)** vertical distribution of PM$_{2.5}$ at 21:30 BT measured at the Hefei site on 17 March 2014.

below 1.8 km a.g.l. with a maximum value of 70 µg m^{-3}, indicating a mild pollutant night in Hefei. Between 0.6 and 1.8 km a.g.l., the PM$_{2.5}$ value is almost constant, indicating a well-mixed layer. The maximum value of PM$_{2.5}$ lies near the Earth surface layer and forms a rather stable aerosol structure, which will cause a hazy day with poor visibility.

It is revealed in Fig. 4d that the PM$_{2.5}$ value remains 20 µg m^{-3} at 0.9–1.8 km a.g.l., and increases to 30 µg m^{-3} at 0.3 km a.g.l., then increases rapidly to a peak of 55 µg m^{-3} at the Earth surface. The vertical distribution of PM$_{2.5}$ at 21:30 BT measured at the Hefei site on 17 March 2014 depicts a stable structure.

Figure 5. (a) RH and T parameters with time, **(b)** K value for each hour, **(c)** time series of PM$_{2.5}$ profile, and **(d)** vertical distribution of PM$_{2.5}$ at 21:00 BT measured at the Hefei site on 13–14 February 2015.

4.3 Case III: Heavy pollutant night

On 13–14 February 2015, it was also cloud-free at night, with the northwest wind of not more than $3\,\mathrm{m\,s^{-1}}$ near the ground. The temperature varies from 10.7 to 9.1 °C with a decreasing trend and the RH increases speedily from 31 to 68 % during the time span of 18:30–02:00 BT, and then keeps around 65 % in the late period of 02:00–05:30 BT as shown in Fig. 5a. The distance D between laser beam and CCD camera is 19.40 m.

Figure 5b plots the hourly mean value of K varying from 0.006 to 0.007 km^{-1} (µg m^{-3}), which also indicates an approximate constant value during this experimental case. But this value is quite different from that obtained from CASE I and CASE II probably due to the differences in aerosol size distribution and refractive index. The PM$_{2.5}$ profile is calculated accordingly by the K value and the aerosol extinction coefficient profile. At the meantime, the spatiotemporal distribution of PM$_{2.5}$ mass concentration for this case at the Hefei site is shown in Fig. 5c. The PM$_{2.5}$ rises to 2.1 km a.g.l. with a maximum value 210 µg m^{-3}, indicating a heavy pollutant night in Hefei. During the observation period, there are three distinct layers (i.e., the floating layer, the clean layer, and the Earth surface layer) with a gradual fall in height from the evening to the next morning. The typical height for the floating layer decreases from 1.2–1.8 to 0.5–1.0 km a.g.l., and the peak value of PM$_{2.5}$ for this layer is about 150 µg m^{-3}. The PM$_{2.5}$ value for the fair layer in middle part varies from 30 to 50 µg m^{-3}. The top height of the Earth surface layer decreases from 0.9 km a.g.l. at 18:00 BT

to 0.3 km a.g.l. at 06:00 BT, which leads to a more stable structure. The maximum value of PM$_{2.5}$ lies near the Earth surface layer, especially below 0.3 km a.g.l., where a high value region of PM$_{2.5}$ (i.e., 200 µg m^{-3} exists all along from 20:00 to 04:00 BT, which will cause a heavy hazy day with worse visibility.

It is noticeable from Fig. 5d that the PM$_{2.5}$ value takes on a sub-peak of 110 µg m^{-3} at 1.2 km a.g.l., and increases rapidly from 20 µg m^{-3} at 0.8 km a.g.l. to another sub-peak of 190 µg m^{-3} at 0.4 km a.g.l., then increases rapidly again to a peak of 210 µg m^{-3} on the Earth surface. The vertical distribution of PM$_{2.5}$ at 21:00 BT measured at the Hefei site on 13–14 February 2015 forms a more stable and rich structure.

In order to validate the new method mentioned above, the comparison of surface PM$_{2.5}$ measured by PM$_{2.5}$ Monitor and C-Lidar is shown in Fig. 6. The values of PM$_{2.5}$ are obtained from the foregoing cases and the slope for the fitting line is 0.995 with a correlative coefficient of 99.8 %, which indicates a good agreement. So, the new method is effective to explore PM$_{2.5}$ profile at the near-ground level when RH is less than 70 %.

5 Summary and conclusion

A new measurement technology of PM$_{2.5}$ mass concentration profile at the near-ground level is presented in this paper based on a CCD side-scatter lidar and a PM$_{2.5}$ detector. Our new method is proved to be effective through the three cases measured during nighttime at the SKYNET Hefei site. And some useful conclusions are drawn as follows.
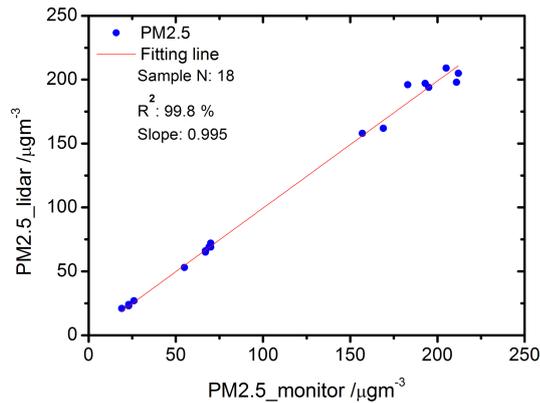
Figure 6. Comparison of surface PM$_{2.5}$ obtained by PM$_{2.5}$ Monitor and C-Lidar.

1. Five types of aerosol from OPAC, prevailing at the Hefei site, are used to testify their extinction coefficient depending on RH, only to indicate seldom reliance on RH when RH is less than 70 %.

2. The specific coefficient K, which is related to aerosol size distribution, refractive index, and atmospheric relative humidity, may contain a fixed value under the suitable condition when RH is less than 70 %, though it may not be the same for each case. So, the PM$_{2.5}$ mass concentration profile can be easily derived from vertical distribution of extinction coefficient for aerosol.

3. The PM$_{2.5}$ is always loading in the planet boundary layer with a multi-layered structure, indicating its complexity of the vertical distribution. And there is a higher lifting height under the heavy-pollution weather condition, demonstrating that air pollution may break through near the surface into a higher altitude and join in further transportation.

4. The high value of PM$_{2.5}$ remains near the ground and forms a stable structure, especially on hazy days, which will cause bad weather conditions, such as low visibility.

5. Our new method for PM$_{2.5}$ mass concentration profile is a useful approach for improving our understanding of air quality and the atmospheric environment, which can also provide critical information for the daily air quality forecast. Further investigation will be carried on in the near future when RH is larger than 70 %, including the potential variation of specific coefficient K.

References

An, J., Zhang, R., and Han, Z.: Seasonal changes of total suspended particles in the air of 15 big cities in northern parts of China, Climatic and Environmental Research, 5, 25–29, 2000.

Bernes, J. E., Bronner, S., and Becket, R.: Boundary layer scattering measurements with a charge-coupled device camera lidar , Appl. Optics, 42, 2647–2652, 2003.

Bo, G., Liu, D., and Wu, D.: Two-wavelength lidar for observation of aerosol optical and hygroscopic properties in fog and haze days, Chinese Journal of Lasers, 41, 0113001, doi:10.3788/cjl201441.0113001, 2014.

Che, H., Xia, X., Zhu, J., Wang, H. Wang, Y., Sun, J., Zhang, X., and Shi, G.: Aerosol optical properties under the condition of heavy haze over an urban site of Beijing, China, Environ. Sci. Pollut. R., 22, 1043–1053, doi:10.1007/s11356-014-3415-5, 2015.

Cordero, L., Wu, Y., Gross, B. M., and Moshary, F.: Use of passive and active ground and satellite remote sensing to monitor fine particulate pollutants on regional scales, Advance environmental, chemical, and Biological sensing technologies IX, Proc. Of SPIE, 8366, 83660M, 2012.

He, X., Deng, Z., Li, C., Lau, A. K., Wang, M., Liu, X., and Mao, J.: Application of MIDIS AOD in surface PM$_{10}$ evaluation, Acta Scientiarum Naturalium Universitatis Pekinensis, 46, 178—184, 2010.

Hess, M., Koepke, P., and Schult, I.: Optical properties of aerosols and clouds: The software package OPAC, B. Am. Meteorol. Soc., 79, 831–844, 1998.

Li, Q., Li, C., Wang, Y., Lin, C., Yang, D., and Li, Y.: Retrieval on mass concentration of urban surface suspended particulate matter with lidar and satellite remote sensing, Acta Scientiarum Naturalium Universitatis Pekinensis, 49, 673—682, 2013.

Ma, X.,Tao, Z., and Ma, M.: The retrival of side-scatter lidar signal based on CCD technique, Acta Optica Sinica, 34, 0201001, doi:10.3788/aos201434.0201001, 2014.

Mao, F., Gong, W., and Li, J.: Geometrical form factor calculation using Monte Carlo integration for lidar, Opt. Laser Technolol., 44, 907–912, 2012.

Mao, J., Zhang, J., and Wang, M.: Summary comment on research of atmospheric aerosol in China, Acta Meteorologica Sinica, 60, 625–634, 2002.

Pesch, M. and Oderbolz, D.: Calibrating a ground based backscatter lidar for continuous measurements of PM$_{2.5}$, lidar technology, techniques, and measurements for atmospheric remote sensing III, Proc. Of SPIE, 6750, 67500K, 2007.

Sano, I., Mukai, M., Okada, Y., Mukai, S., Sugimoto, N., Matsui, I., Shimizu, A.: Improvement of PM$_{2.5}$ analysis by using AOT and lidar data Remote sensing of the atmospheric and clouds U, Proc. Of SPIE, 7152, 71520M, 2008.

Tao, Z., Liu, D., and Ma, X.: Development and case study of side-scatter lidar system based on charge-coupled device, Infrared and Laser Engineering, 43, 3282–3286, 2014a.

Tao, Z., Liu, D., and Wang, Z.: Measurements of aerosol phase function and vertical backscattering coefficient using a charge-coupled device side-scatter lidar, Opt. Express, 22, 1127–1134, doi:10.1364/OE.22.001127, 2014b.

Tao, Z., Liu, D., Ma, X., Shi, B., Shan, H., and Zhao, M.: Vertical distribution of near-ground aerosol backscattering coefficient measured by a ccd side-scattering lidar, Appl. Phys. B, 120, 631–635, 2015.

Wang, Z., Liu, D., Wang, Z., Wang, Y., Khatri, P., Zhou, J., Takamura, T., and Shi, G.: Seasonal characteristics of aerosol optical properties at the SKYNET Hefei site (31.90° N, 117.17° E) from 2007 to 2013, J. Geophys. Res.-Atmos., 119, 6128–6139, doi:10.1002/2014JD021500, 2014a.

Wang, Z., Liu, D., and Cheng, Z.: Pattern recognition model for haze identification with atmospheric backscatter lidars, Chinese Journal of Lasers, 41, 1113001, doi:10.3788/cjl201441.1113001, 2014b.

Wang, Z., Liu, D., Wang, Y., Wang, Z., and Shi, G.: Diurnal aerosol variations do affect daily averaged radiative forcing under heavy aerosol loading observed in Hefei, China, Atmos. Meas. Tech., 8, 2901–2907, doi:10.5194/amt-8-2901-2015, 2015a.

Wang, Z., Tao, Z., Liu, D., Wu, D., Xie, C., and Wang, Y.: New experimental method for lidar overlap factor using a CCD side-scatter technique, Opt. Lett., 40, 1749–1752, 2015b.

Weitkamp, C.: Lidar: Range-Resolved Optical Remote Sensing of the Atmosphere, Springer, New York, USA, 2005.

Winker, D., Hunt, W., and McGill, M.: Initial performance of assessment of CALIOP, Geophys. Res. Lett., 34, L19803, doi:10.1029/2007GL030135, 2007.

Wu., Z., Liu, A., and Zhang, C.: Vertical distribution feature of PM$_{2.5}$ and effect of boundary layer in Tianjin, Urban Environment & Urban Ecology, 22, 24–29, 2009.

Xu, J., Ding, G., and Yan, P.: Componential characteristics and sources identification of PM$_{2.5}$ in Beijing, Journal of Applied Meteorological Science, 18, 645–654, 2007.

Yang, L., He, K., and Zhang, Q.: Vertical distributive characters of PM$_{2.5}$ at the ground layer in Autumn and Winter in Beijing, Research of Environmental Sciences, 18, 23–28, 2005.

Zhou, J., Yu, G., Jin, C., Qi, F., Liu, D., Hu, H., Gong, Z., Shi, G., Nakajima, T., and Takamura, T.: Lidar observations of Asian dust over Hefei, China, in spring 2000, J. Geophys. Res., 107, AAC5.1–AAC5.8, doi:10.1029/2001JD000802, 2002.